Minerals Engineering 117 (2018) 108–116

Contents lists available at ScienceDirect

Minerals Engineering

journal homepage: www.elsevier.com/locate/mineng

Discrete modelling of the compaction of non-spherical particles using a multi-sphere approach

Y. He[a], T.J. Evans[b], Y.S. Shen[c], A.B. Yu[d], R.Y. Yang[a,*]

[a] School of Materials Science and Engineering, University of New South Wales, Sydney 2052, Australia
[b] Rio Tinto Iron Ore Group, Australia
[c] School of Chemical Engineering, University of New South Wales, Sydney 2052, Australia
[d] Department of Chemical Engineering, Monash University, Clayton 3900, Australia

ARTICLE INFO

Keywords:
Compaction
Non-spherical particles
Discrete element method
Compact strength

ABSTRACT

A numerical model based on the discrete element method (DEM) was developed to study the compaction behaviour of non-spherical particles. Spheroidal and tetrahedral particles of different aspect ratios were approximated by a multi-sphere approach in which overlapping spheres were glued together to represent the particle shapes. For the compactions of spheroidal particles, the effect of aspect ratio on the compaction was mainly due to the difference in the initial packing. The compact compressive strength also increased with the aspect ratio. For the tetrahedral particles, the non-convexity shape index was proposed to represent the degree of inter-particle locking. With increasing non-convexity and thus inter-particle locking, larger consolidation pressure was required to achieve the same density. The failure region upon the unconfined pressure also moved from the bottom to the top with increasing non-convexity as force transfer was more difficult in the compacts. The simulations also indicated that the bulk failure of the compacts was dominated by the shear-induced bond breakage. The findings facilitate a better understanding of the relation of particle shape to the compaction behaviour and compact strength.

1. Introduction

Preparation, transportation, storage, and associated operations may account for 30–60% of the total delivered price of raw material in the mining and mineral processing industry (Wills and Napier-Munn, 2006). Compaction is an important operation to consolidate ore fines into assembled products for better handling with reduced cost. The physical and mechanical properties of a compact are critical to the performance of the compact in the following operations and applications such as transport, storage and sintering (Alderborn et al., 1988; Darvell, 1990; Fell and Newton, 1970; Podczeck, 2012). Better understanding the relationship between consolidation pressure and compact properties is critical to the design and optimisation of the process (Abdel-Ghani et al., 1991).

Numerical modelling based on the discrete element method (DEM) has been used to link the microscopic interactions between particles with the macroscopic property of a compact, such as the effect of mechanical properties of particles (Hassanpour and Ghadiri, 2004; Samimi et al., 2005), particle-wall friction induced inhomogeneity (Foo et al., 2004), evolution of compact structure (Sheng et al., 2004) and the effects of moisture, particle shape and particle size (Skrinjar and Larsson, 2004, 2012; Thakur et al., 2014). Recently we conducted a DEM study of the compressive strength of iron ore compacts (He et al., 2017; He et al., 2015). The simulated stress-strain responses were comparable with those observed from the physical experiments. As the DEM treats particles individually and explicitly considers the particle characteristics, material properties and the inter-particle forces, it offers an efficient way to obtain micro-mechanical insight into the bulk behaviour of compaction.

In mineral processing, ore particles are often non-spherical and particle shape has been demonstrated to have a strong influence on the mechanical behaviour in particle packing (Donev et al., 2004; Villarruel et al., 2000), compaction (Rothenburg and Bathurst, 1992; Ting et al., 1995) and flow Cleary and Sawley, (2002). For example, in the biaxial compression of elliptical particles, much larger strength was observed compared to that of disk-shaped particles (Rothenburg and Bathurst, 1992). Ting et al. (1995) observed that the shear strength of a 2D assembly of ellipse shaped particles increased with particle angularity. The enhanced shear strength was attributed to the rolling resistance due to particle inter-locking. Chung and Ooi (2006) obtained a better agreement with experimental results in the bulk response when the particle shape was considered under confined compression. Recently,

* Corresponding author.
E-mail address: r.yang@unsw.edu.au (R.Y. Yang).

https://doi.org/10.1016/j.mineng.2017.12.013
Received 19 June 2017; Received in revised form 18 October 2017; Accepted 13 December 2017

Wiacek et al. (2012) observed that the transfer of the vertical pressure was sensitive to the aspect ratio of elongated particles in the uniaxial compression. However, little effort has been devoted to investigating the mechanical response and strength of non-spherical particle compacts under the unconfined axial compression.

This study is to develop a DEM model to study the compaction of two types of non-spherical particles, spheroidal and tetrahedral particles, of different shape factors. The focus will be mainly on the effect of particle shape on compact structure and strength. A multi-sphere approach is used to approximate the particle geometry. The model is firstly validated against the literature data and then extended to study their behaviour in the die and unconfined compactions.

2. Model description

The translational motion of a non-spherical particle i with mass m_i and inertial tensor $\mathbf{I}_i$ is defined based on its mass centre and the rotational motion obeys the Euler equations in body-fixed coordination system, given by,

$$m_i \frac{d\mathbf{v}_i}{dt} = \mathbf{F}_i + m_i\mathbf{g} \tag{1}$$

$$\mathbf{I}_i \frac{d\omega_i}{dt} + \omega_i \times (\mathbf{I}_i\omega_i) = \mathbf{M}_i \tag{2}$$

where $\mathbf{v}_i$ and ω_i are, respectively, the translational and angular velocity with respect to the mass centre. $\mathbf{F}_i$ is the sum of all externally applied force acting on the particle, including the normal contact force $\mathbf{F}_{ij}^n$, tangential contact force $\mathbf{F}_{ij}^t$, capillary force $\mathbf{F}_{ij}^{cap}$ and the bonding forces $\mathbf{F}_{ij}^b$ when a bond is present between the two particles. $\mathbf{g}$ is the gravity acceleration. $\mathbf{M}_i$ is the corresponding moment, including the moment $\mathbf{M}_{ij}^t$ caused by tangential force and the moment $\mathbf{M}_{ij}^b$ induced by the tangential bonding force and bond bending/torsion. Fig. 1 shows the schematic illustration of forces between elemental spheres.

The particles are modelled as an elastic-perfectly plastic body. The normal contact is described by the Hertz model for the elastic deformation and the model developed by Thornton and Ning (1998) for the plastic deformation. The tangential contact behaviour is governed by the model of Mindlin and Deresiewicz (1953). A bonded particle model (Potyondy and Cundall, 2004) was adopted to account for the effect of solid bonding and mechanic interlocking due to its simple, linear form which can be easily implemented into the model. More importantly, the model has been demonstrated to be able to reproduce the brittle fracture observed in the experiments (Cho et al., 2007; Yoon, 2007). In the present study, the bonding area is assumed to be the same as contact area between the particles. The bonds can be broken by either tensile or shear.

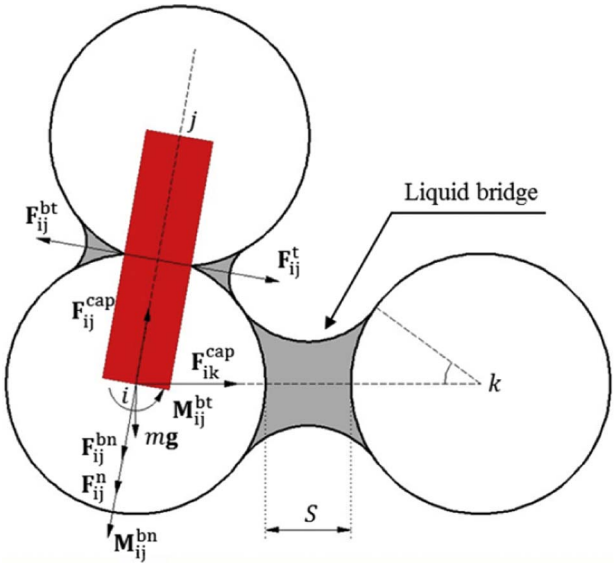

Fig. 1. Schematic of the forces acting on sphere i from contacting sphere j and pendular liquid-bridge linked sphere k.

For non-spherical particles, the calculation of the mass and the moment of inertial tensor relative to the principal axes are very complex. In the present study, they are obtained using *SolidWorks*, a *CAD* software and fed into the DEM model as input parameters. To avoid updating the moment of inertia, the torques and angular velocities are transformed between the space-fixed coordination system and the body-fixed coordinate system via a transformation matrix which is defined by the Euler angles (ϕ,θ,ψ) as,

$$\mathbf{A} = \begin{pmatrix} \cos\phi\cos\psi - \sin\phi\cos\theta\sin\psi & \sin\phi\cos\psi + \cos\phi\cos\theta\sin\psi & \sin\theta\sin\psi \\ -\cos\phi\sin\psi - \sin\phi\cos\theta\cos\psi & -\sin\phi\sin\psi + \cos\phi\cos\theta\cos\psi & \sin\theta\cos\psi \\ \sin\phi\sin\theta & -\cos\phi\sin\theta & \cos\theta \end{pmatrix} \tag{3}$$

To determine the rotational motion, the so-called quaternion method are used to represent the particle orientation to avoid the problem of gimbal lock involved in the calculation of the Euler angle (Dziugys and Peters, 2001).

Table 1 lists the equations used for the calculation of these forces. The details can be found in our previous study (He et al., 2015).

3. Simulation conditions

This work investigated the compactions of spheroidal (Fig. 2) and tetrahedral (Fig. 3) particles. The particle shape was approximated using a multi-sphere approach, in which the elemental spheres are rigidly connected so that the contact detection method for spherical particles can be readily adopted (Favier et al., 1999). Each elemental sphere was defined by its radius and position relative to the mass centre of the particle. The contact detection between non-spherical particles is

Table 1
Equations used to calculate forces in this work.

Force	Equation
Normal contact force	$\mathbf{F}_{ij}^n = \begin{cases} \frac{4}{3}E^*R^{*1/2}\delta_n^{3/2}\hat{\mathbf{n}}_{ij} & (\delta < \delta_y) \\ [F_y + \pi p_y R^*(\delta-\delta_y)]\hat{\mathbf{n}}_{ij} & (\delta \geqslant \delta_y) \end{cases}$
Tangential contact force	$\mathbf{F}_{ij}^t = -\frac{\delta_t\mu_t \mid \mathbf{F}_{ij}^n\mid}{\mid\delta_t\mid}\left[1-\left(1-\frac{\min(\mid\delta_t\mid,\delta_{t,max})}{\delta_{t,max}}\right)^{3/2}\right]$
Capillary force	$\mathbf{F}_{ij}^{cap} = \begin{cases} \frac{2\pi R^*\gamma\cos\theta_c}{1+1/[\sqrt{1+2V_L/(\pi R^{*2})}-S]}\hat{\mathbf{n}}_{ij} & (\text{P-P}) \\ \frac{4\pi R^*\gamma\cos\theta_c}{1+S/\sqrt{\pi R^*/V_L}}\hat{\mathbf{n}}_{ij} & (\text{P-W}) \end{cases}$
Particle-bonding force	$\{\Delta\mathbf{F}_{ij}^b\} = -\{\mathbf{K}\}\{\Delta\mathbf{x}\}$, the criteria for bond breakage are given by, $\min\left(\frac{-\mathbf{F}_{ij}^{bn}}{A}+\frac{\mid\mathbf{M}_{ij}^{bt}\mid R_b}{I},\frac{\mid\mathbf{F}_{ij}^{bt}\mid}{A}+\frac{\mid\mathbf{M}_{ij}^{bn}\mid R_b}{J}\right) \geqslant \sigma_b$
Moment due to tangential force	$\mathbf{M}_{ij}^t = \mathbf{F}_{ij}^t \times \mathbf{R}_i$
Rolling moment	$\mathbf{M}_{ij}^r = \mu_r R_i \mid\mathbf{F}_{ij}^n\mid\hat{\omega}_i$

where $1/R^* = 1/R_i + 1/R_j$, with R_i and R_j being the radius of two particles in contact, $1/E^* = (1-\nu_i^2)/E_i + (1-\nu_j^2)/E_j$, with E and ν the Young's Modulus and Poisson's ratio, respectively; δ_n and δ_t represent the overlap in normal and tangential directions; $\delta_{t,max} = 3\mu_t\mid\mathbf{F}_{ij}^n\mid/16G^*a$ with μ_t the sliding friction, a the radius of contact area and G^* is the effective shear modulus defined as $G^* = E^*(1-\nu)/(4-2\nu)$; μ_r is the rolling friction; $\hat{\omega}_i = \omega_i/|\omega_i|$ with ω_i the angular velocity; For inter-particle bonding, $\{\Delta\mathbf{F}_{ij}^b\} = \{\Delta F_{ij}^{bn},\Delta F_{ij}^{bt},\Delta M_{ij}^{bn},\Delta M_{ij}^{bt}\}^T$ and $\{\Delta\mathbf{x}\} = \{\Delta\delta^n,\Delta\delta^t,\Delta\theta^n,\Delta\theta^t\}^T$ are, respectively, the incremental force vector and the incremental displacement vector. $\{\mathbf{K}\} = \{k^nA,k^tA,k^tJ,k^nI\}^T$ is the stiffness matrix, in which k^n and k^t are the bond normal and tangential stiffness, $A = \pi R_b^2$, $I = \pi R_b^4/4$ and $J = \pi R_b^4/2$ with R_b the bonding radius and σ_b the bonding strength.